Moving Horizon Observer for Vibration Dynamics with Plant Uncertainties in Nanopositioning System Estimation

Tomáš Polóni, Arnfinn Aas Eielsen, Boris Rohaľ-Ilkiv and Tor Arne Johansen

***Abstract*— This paper considers the estimation of states and parameters of a Single-Degree-of-Freedom (SDOF) vibration model in nanopositioning system based on a nonlinear Moving Horizon Observer (MHO). The MHO is experimentally tested and verified on measured data. The information about the displacement and speed together with the system parameters and unmodeled force disturbance is estimated through the Sequential Quadratic Programming (SQP) optimization procedure. The MHO provided superior performance in comparison with the benchmark method Extended Kalman Filter (EKF) in terms of faster convergence.**

I. INTRODUCTION

Improvement of machine precision motivates the development of new solutions for canceling the noise and vibrations. The nanopositioning is a state of art of precise mechanics where the vibration attenuation and control problems challenge the computational hardware and software as well as overall mechatronic design [1]. Model-based controllers depend on parametric models where the states and parameters can be estimated through observers.

The classical on-line approach to determine the state and parameters is in vibration mechanics the Kalman filter and its modified version for nonlinear systems, the Extended Kalman Filter (EKF) [2]. The foundation of such filtration is the model of the vibrating structure based on the lumped parameter model assumption [3]. The typical application of filtration of state and parameters is the control [4], diagnostics and monitoring of vibrating system [5]. The EKF provides sub-optimal estimates due to the linearization, and additional sub-optimality follows from model errors and violation of the Gaussian white noise assumption. Moreover, the method is sensitive to the initial condition and may not converge.

The objective and novel contribution of this study is the experimental application of nonlinear least-squares estimation of states, parameters and force disturbance of nanopositioning device with MHO [6]. While the EKF accumulates past history measurement information in the a priori estimate of the state and the error covariance matrix estimate, the MHO uses finite moving horizon data window to extract the information from the actually measured and past measured data. The MHO [7], [8] is the alternative to particle filter statistical methods (PF) [9], [10] and minimum-variance (EKF) methods. The paper compares the MHO performance with the EKF.

This work is supported by the Slovak Research and Development Agency under projects APVV-0090-10 and LPP-0118-09. This work is also supported by the Norwegian Research Council and the Norwegian University of Science and Technology.

Tomáš Polóni tomas.poloni@stuba.sk and Boris Rohaľ-Ilkiv boris.rohal-ilkiv@stuba.sk are with the Institute of Automation, Measurement and Applied Informatics at the Faculty of Mechanical Engineering, Slovak University of Technology, Bratislava, Slovakia

Arnfinn Aas Eielsen eielsen@itk.ntnu.no and Tor Arne Johansen tor.arne.johansen@itk.ntnu.no are with the Department of Engineering Cybernetics at the Norwegian University of Science and Technology, Trondheim, Norway

II. BASIC MODEL FORMULATION

The structural vibration model can be written as

$$M_0\ddot{q} + C_0\dot{q} + K_0 q \quad = \quad L_0 f_0 \tag{1}$$

where M_0 is the mass matrix, C_0 is the damping matrix, K_0 is the stiffness matrix, L_0 is the transition matrix, q is the displacement vector and f_0 is the excitation force. It consists of known force input f and unknown force input f_u and is written as $f_0 = [f, f_u]^T$. The transition matrix L_0 consists of the transition matrix for known force input L and transition matrix for unknown force input L_u, $L_0 = [L, L_u]$. The applied forces through the actuators are modeled as $f = Cu$, where the matrix $C = diag(c)$, the vector of gain parameters of the actuators is $c \in \mathbb{R}^{n_c}$ and $u \in \mathbb{R}^{n_u}$ is the vector of input variables of the actuators. Conventionally, the state-space equation can be represented as

$$\dot{x}_s \quad = \quad Ax_s + Bu + w \tag{2}$$

where $x_s = \begin{bmatrix} q \\ \dot{q} \end{bmatrix}$, $A = \begin{bmatrix} 0 & I \\ -M_0^{-1}K_0 & -M_0^{-1}C_0 \end{bmatrix}$, $B = \begin{bmatrix} 0 \\ M_0^{-1}LC \end{bmatrix}$, $G = \begin{bmatrix} 0 \\ M_0^{-1}L_u \end{bmatrix}$, $w = Gf_u$

An augmented state vector $x \in \mathbb{R}^{2n_q+n_p}$ can be defined

$$x = [x_s, p]^T = [q, \dot{q}, p_p, c, w]^T \tag{3}$$

where $p \in \mathbb{R}^{n_p}$ is the vector of uncertain model parameters p_p (e.g. stiffness, damping parameters), unknown gain parameters c and unknown state disturbances w. The number of modes is n_q, and n_p is the total number of unknowns to be identified. A common procedure is to include a process noise vector in Eq. (2) which accounts for random and unmodeled behavior. For the purpose of state estimation and parameter identification the vibration dynamics (1) is described by general time-invariant augmented state-space equations

$$\dot{x}_s \quad = \quad \tilde{f}_c(x_s, p, u) + z_s \tag{4}$$

$$\dot{p} \quad = \quad z_p \tag{5}$$

where $\tilde{f}_c : \mathbb{R}^{2n_q} \times \mathbb{R}^{n_p} \times \mathbb{R}^{n_u} \rightarrow \mathbb{R}^{2n_q}$ is given by $\tilde{f}_c(x_s, p, u) = A(p_p)x_s + B(c)u + w$. The state process noise vector is $z_s \in \mathbb{R}^{2n_q}$ and the parameter process noise vector is

$z_p \in \mathbb{R}^{n_p}$.The model which was linear-in-the-states becomes nonlinear by declaring the unknown model parameters as additional states of the system.

Eq. (4) and (5) can be combined as

$$\dot{x} = f_c(x, u) + z \tag{6}$$

where $f_c : \mathbb{R}^{2n_q+n_p} \times \mathbb{R}^{n_u} \rightarrow \mathbb{R}^{2n_q+n_p}$ represents the augmented dynamics and $z = [z_s, z_p]^T$. The observation equation may be written as

$$y = h_c(x, u) + v \tag{7}$$

where $y \in \mathbb{R}^{n_y}$ is a vector of measurements and $h_c : \mathbb{R}^{2n_q+n_p} \times \mathbb{R}^{n_u} \rightarrow \mathbb{R}^{n_y}$ is a continuous measurement function. The measurement errors are modeled with the noise term $v \in \mathbb{R}^{n_y}$. The most frequent situation encountered in practice is when the system is governed by continuous-time dynamics and the measurements are obtained at discrete time instances. For the problem formulation we consider the numerically discretized dynamic nonlinear system described by the equations

$$x_{t+1} = f(x_t, u_t) + z_t \tag{8}$$
$$y_t = h(x_t, u_t) + v_t \tag{9}$$

for $t = 0, 1, \ldots$, where $x_t \in \mathbb{R}^{n_x}$ is the augmented state vector, $u_t \in \mathbb{R}^{n_u}$ is the input vector and $z_t \in \mathbb{R}^{n_x}$ is the process noise vector. The state vector is observed through the measurement equation (9) where $y_t \in \mathbb{R}^{n_y}$ is the observation vector and $v_t \in \mathbb{R}^{n_y}$ is a measurement noise vector.

III. Extended Kalman Filter

The EKF is perhaps the most often applied algorithm for the estimation of state and parameters of nonlinear dynamic systems [2] and it will be considered here as the benchmark algorithm. The following algorithm is in the literature known as continuous-discrete or hybrid EKF [2]. The dynamic system is given by (8) and (9). The main assumption about the process and the measurement noise is that they have the white noise properties, i. e. sequentially uncorrelated Gaussian distribution with zero mean

$$z_t \sim N(0, Q_t) \qquad v_t \sim N(0, R_t) \tag{10}$$

where Q_t is a process noise covariance matrix and R_t is a measurement noise covariance matrix. The initial condition of the state vector is $x_0 \sim N(\hat{x}_0^+, P_0^+)$. The estimate of the state vector at $t = 0$ begins with the initial state vector estimate and with the initial covariance matrix of the initial state vector estimation error

$$\hat{x}_0^+ = E[x_0] \tag{11}$$
$$P_0^+ = E[(x_0 - \hat{x}_0^+)(x_0 - \hat{x}_0^+)^T] \tag{12}$$

From time instance $t-1$, the dynamic system (6) is simulatively propagated one step ahead as

$$\hat{x}_t^- = f(\hat{x}_{t-1}^+, u_{t-1}) \tag{13}$$

where $t = 1, 2, \ldots$. This one step prediction gives an a priori state estimate. The time update of the covariance matrix estimate is given by

$$\dot{P} = Z(\hat{x})P + PZ^T(\hat{x}) + Q \tag{14}$$

where

$$Z(\hat{x}) = \left.\frac{\partial f_c(x)}{\partial x}\right|_{x=\hat{x}} \tag{15}$$

and Q is a spectral density matrix, where $Q = \frac{1}{T}Q_t$. The covariance matrix estimate of state vector $\hat{x}_t^-$ estimation error is achieved by simulative propagation of Eq. (14)

$$P_t^- = g(P_{t-1}^+, Z(\hat{x}_{t-1}^+)) \tag{16}$$

The EKF gain matrix is in time instant t

$$K_t = P_t^- L_t^T [L_t P_t^- L_t^T + M_t R_t M_t^T]^{-1} \tag{17}$$

and the measurement y_t is used for state vector estimation (a posteriori estimate)

$$\hat{x}_t^+ = \hat{x}_t^- + K_t[y_t - h(\hat{x}_t^-)] \tag{18}$$

The covariance matrix a posteriori estimate is updated as

$$P_t^+ = [I - K_t L_t]P_t^-[I - K_t L_t]^T + K_t M_t R_t M_t^T K_t^T \tag{19}$$

where

$$L_t = \left.\frac{\partial h(x_t)}{\partial x_t}\right|_{x_t=\hat{x}_t^-} \tag{20}$$

$$M_t = \left.\frac{\partial h(x_t)}{\partial v_t}\right|_{x_t=\hat{x}_t^-} \tag{21}$$

The presented EKF algorithm will be generally noticed as

$$\hat{x}_{t+1}^+ = f_F(y_{t+1}, \hat{x}_t^+, u_t) \tag{22}$$

for $t = 0, 1, \ldots$, where $f_F : \mathbb{R}^{2n_q+n_p} \times \mathbb{R}^{n_u} \rightarrow \mathbb{R}^{2n_q+n_p}$ represents the EKF dynamics and its shorter notation $f_F^{u_t}(\cdot)$ will be used.

IV. Moving horizon observer algorithm

In the basic moving horizon estimation formulation the statistics of the process and measurement noises z_t, v_t are assumed unknown. The function composition as the application of one function to the results of another like $f(f(x_{t-N}, u_{t-N}), u_{t-N+1})$ and $h(f(x_{t-N}, u_{t-N}), u_{t-N+1})$ can be written as $f^{u_{t-N+1}} \circ f^{u_{t-N}}(x_{t-N})$ and $h^{u_{t-N+1}} \circ f^{u_{t-N}}(x_{t-N})$ respectively, where "$\circ$" denotes function composition. The $N+1$ subsequent measurements of the outputs Y_t and inputs U_t up to time t with the $N+1$ measurement noise vector V_t is

$$Y_t = \begin{bmatrix} y_{t-N} \\ y_{t-N+1} \\ \vdots \\ y_t \end{bmatrix}; U_t = \begin{bmatrix} u_{t-N} \\ u_{t-N+1} \\ \vdots \\ u_t \end{bmatrix}; V_t = \begin{bmatrix} v_{t-N} \\ v_{t-N+1} \\ \vdots \\ v_t \end{bmatrix} \tag{23}$$

where $t = N+1, N+2, \ldots$. Neglecting process noise in the basic MHO formulation, following algebraic map is defined

$$H_t(x_{t-N}, U_t) = \begin{bmatrix} h^{u_{t-N}}(x_{t-N}) \\ h^{u_{t-N+1}} \circ f^{u_{t-N}}(x_{t-N}) \\ \vdots \\ h^{u_t} \circ f^{u_{t-1}} \circ \ldots \circ f^{u_{t-N}}(x_{t-N}) \end{bmatrix}$$
$$Y_t = H_t(x_{t-N}, U_t) + V_t \quad (24)$$

Define the N-information vector at time t

$$I_t = [y_{t-N}^T, \ldots, y_t^T, u_{t-N}^T, \ldots, u_t^T]^T \quad (25)$$

The observer design problem is to reconstruct the vector x_{t-N} based on the information vector I_t. The basic formulation of such a problem is defined as the inverse mapping of Eq. (24). The unique existence and continuity of the solution depends on the function H_t. If the Eq. (24) does not have unique solution, the problem is ill-posed according to definitions of [11]. The solution of vector x_{t-N} is in the case of uniform observability formulated on an over-determined set of algebraic equations where there are more equations than unknowns for which $n_x \leq N n_y$. The formulation can be under-determined if there is no persistence of excitation, or the system is not observable [7].

The cost function of the MHO optimization problem is in the meaning of the least-squares method defined as

$$J_{LS}(\hat{x}_{t-N|t}, I_t) = \|\hat{x}_{t-N|t} - \bar{x}_{t-N|t}\|_S^2 + \alpha \|\hat{Y}_t - Y_t\|^2 \quad (26)$$

subject to the state constraints

$$\hat{x}_{t-N}^{min} \leq \hat{x}_{t-N} \leq \hat{x}_{t-N}^{max} \quad (27)$$

where

$$\hat{Y}_t = H_t(\hat{x}_{t-N}, U_t) = \begin{bmatrix} h^{u_{t-N}}(\hat{x}_{t-N}) \\ h^{u_{t-N+1}} \circ f^{u_{t-N}}(\hat{x}_{t-N}) \\ \vdots \\ h^{u_t} \circ f^{u_{t-1}} \circ \ldots \circ f^{u_{t-N}}(\hat{x}_{t-N}) \end{bmatrix} \quad (28)$$

The cost function (26) comprises of two squared norms where the first norm is weighted by the S matrix. The contribution of the N-step model response to the optimized vector $\hat{x}_{t-N}$ is expressed through the second norm weight parameter α. The first term in the given formulation can be used to estimate the arrival cost [8], [12].

The a priori state estimate used in the arrival cost at the beginning of the horizon is declared as $\bar{x}_{t-N|t}$ and is computed in a time instant t for the time instance $t-N$ by pre-filtration with an EKF [12]. The EKF is running at the beginning of horizon on the output data y_{t-N} which were measured in the $t-N$ time instance. This is the information which corrects the one-step simulation

$$\hat{x}_{t-N|t}^- = f(\hat{x}_{t-N-1|t-1}, u_{t-N-1}) \quad (29)$$

The a priori state estimate at the beginning of the horizon is computed as

$$\bar{x}_{t-N|t} = \hat{x}_{t-N|t}^- + K_{t-N|t}[y_{t-N} - h(\hat{x}_{t-N|t}^-)] \quad (30)$$

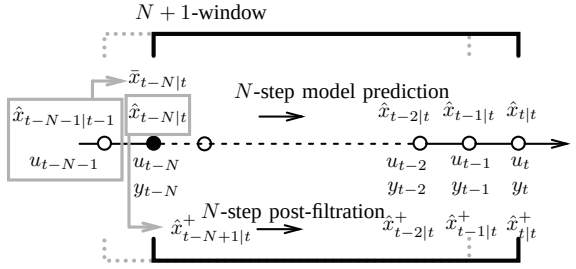

Fig. 1. Time sequences of state, input and output variables in $N+1$ Moving Horizon window

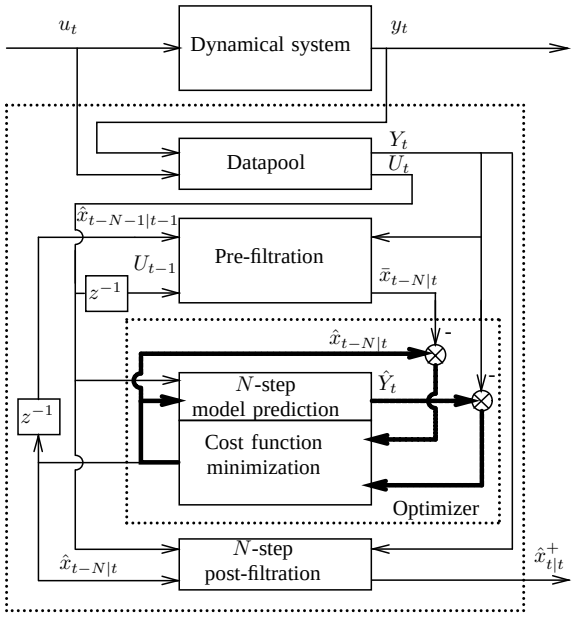

Fig. 2. Algorithm scheme of Moving Horizon Observer where z^{-1} is a one sample delay operator

The covariance matrix is computed according to Eq. (31). The other matrix computations necessary for the pre-filtration are done via regular EKF equations as explained in Section III (index t changes to $t-N|t$ and index $t-1$ changes to $t-N-1|t-1$). The only difference is that the EKF equations here are applied for the first time instance $t-N$ of receding window. Note that with this pre-filtration the stochastic properties of the process noise and measurement noise is assumed known. Also note that neglecting process noise in (28) may lead to accuracy loss, and is made for reduced computations. The post-filtration is further performed to propagate the state to current time instance t.

The schematic time sequence of the a priori state estimate vector $(\bar{x})$, state estimate vectors $(\hat{x})$, post-filtered state estimate vectors $(\hat{x}^+)$, input (u) and output (y) vectors on N-horizon are in Figure 1. The MHO algorithm, schematically shown in Figure 2 consists of three main computation parts: Pre-filtration, Optimizer, and N-step post-filtration. The Optimizer contains N-step model simulation and Cost function minimization blocks. The main computation engine is the optimization algorithm that performs the cost function minimizations. The MHO algorithm with pre-filtration can

$$P^{+}_{t-N|t} = [I - K_{t-N|t}L_{t-N|t}]P^{-}_{t-N|t}[I - K_{t-N|t}L_{t-N|t}]^T + K_{t-N|t}M_{t-N|t}R_tM^T_{t-N|t}K^T_{t-N|t} \quad (31)$$

be summarized into following steps:

St. 0. Load the initial Datapool with measurement data and input data

St. 1. Obtain the actual output measurement y_t, input u_t and update the Datapool

St. 2. If the current time instance is $t = N + 1$, set the initial values for $\hat{x}^{+}_{0|N}$ and $P^{+}_{0|N}$ (as in the case of EKF Eq. (11),(12)). Then according to Figure 1: $\hat{x}^{+}_{0|N} = \hat{x}_{0|N}$ (this value is set by the user)
Else for $t > N + 1$: $\hat{x}^{+}_{t-N-1|t-1} = \hat{x}_{t-N-1|t-1}$ (this value is set from the last optimization run)

St. 3. Compute the a priori estimate with Eq. (29)

St. 4. Numerically integrate $P^{-}_{t-N|t}$ (as in the case of EKF Eq. (14) through Eq. (16))

St. 5. Compute the EKF gain matrix $K_{t-N|t}$ (as in the case of EKF according to Eq. (17))

St. 6. Compute the a posteriori state estimate $\hat{x}^{+}_{t-N|t}$ with Eq. (30) where $\hat{x}^{+}_{t-N|t} = \bar{x}_{t-N|t}$ (Block in Figure 2: Pre-filtration)

St. 7. Minimize the cost function (26) to numerically compute the optimal state vector at the very beginning of receding window $\hat{x}_{t-N|t}$. In the minimization routine the model is used through the Eq. (28). The initial condition for the optimization is $\hat{x}^{init}_{t-N|t} = \bar{x}_{t-N|t}$.

St. 8. Use the EKF to estimate the state from the beginning of receding window to the end of receding window as

$$\hat{x}^{+}_{t-N+i|t} = f_F^{u_{t-N+(i-1)}}(y_{t-N+i}, \hat{x}^{+}_{t-N+(i-1)|t}), \quad (32)$$

where $i = 1, 2, \ldots, N$. The initial condition for the first step ($i = 1$) is $\hat{x}^{+}_{t-N|t} = \hat{x}_{t-N|t}$. (Block in Figure 2: N-step post-filtration)

End of loop; Go to Step 1.

The numerical nonlinear programming solver will be discussed later in the context of the experiment.

V. ODE SOLVER USED BY EKF AND MHO

In both studied approaches (EKF, MHO), the propagation of filter dynamics in Eq. (13), (14) and the propagation of observer dynamics in Eq.(29), (28) is required through the numerical simulation. Since variable-step solvers cannot be used for hard real-time applications required to maintain a fixed processing time, this study is based on fixed-step solvers. Any of the fixed-step continuous solvers can simulate a model to any desired level of accuracy, given a small enough step size. Unfortunately, it generally is not possible, or at least not practical, to decide a priori which combination of solver and step size will yield acceptable results for the continuous states in the shortest time. Determining the best solver for a particular model generally requires experimentation. In the following experiments the Matlab function `ode2` is used (the explicit Heun's method). The `ode2` procedure for calculating the numerical solution to the initial value problem defined by the deterministic part of Eq. (6) $\dot{x} = f_c(x, u)$ with the initial condition x_0 is

$$\tilde{x}_{i+1} = x_i + hf_c(x_i, u_i) \quad (33)$$

$$x_{i+1} = x_i + \frac{h}{2}(f_c(x_i, u_i) + f_c(\tilde{x}_{i+1}, u_i)) \quad (34)$$

where i represents the numerical step index and h is the numerical step size. It can be seen as an extension of the Euler method into a two-stage second-order Runge-Kutta method. Heun's method is a predictor-corrector method with forward Euler's method as predictor Eq. (33) and trapezoidal method as corrector Eq. (34) [13]. This method was chosen after some experimentation with a set of solvers. The precision of the numerical solution of a given solver as a function of numerical step size h is evaluated during the run of the EKF. In our case, the solver which gives the best EKF performance (smallest filtration errors) with other EKF settings unchanged, is chosen.

VI. EXPERIMENTS

The presented MHO algorithm is experimentally tested on the transient vibration motion data from the nano-positioning stage shown in Figure 3. The system dynamics is perturbed by the force generated in piezoelectric actuators forcing the stage to move and vibrate around constant reference displacement value. The transient vibration is triggered by sudden removal of the payload (of a priori unknown weight) attached to the vibrating system which is being excited by the actuator force. The goal is to estimate the state-space vibration model around the first resonant frequency of the system, before and after the removal of payload and also during the transient.

A. Model of Mass-Spring-Damper system

For a Single-Degree-of-Freedom vibration system (SDOF), the equation of motion may be represented as follows

$$m\ddot{q}(t) + b\dot{q}(t) + kq(t) = f_0(t) \quad (35)$$

The state-space model consists of an ordinary differential equation system with the mass m [kg], displacement $q = x_1$ [μm], speed $\dot{q} = x_2$ [μm.s^{-1}], external force $f = cu$ [kg.μm.s^{-2}] applied through the piezoelectric actuator and unknown force disturbance f_u [kg.μm.s^{-2}]

$$\begin{bmatrix} \dot{x}_1 \\ \dot{x}_2 \end{bmatrix} = \begin{bmatrix} 0 & 1 \\ -\frac{k}{m} & -\frac{b}{m} \end{bmatrix} \begin{bmatrix} x_1 \\ x_2 \end{bmatrix} + \begin{bmatrix} 0 \\ \frac{c}{m} \end{bmatrix} u + \begin{bmatrix} 0 \\ \frac{1}{m} \end{bmatrix} f_u \quad (36)$$

The voltage input for the piezoelectric actuator is u [V] and the state vector is $x = [x_1, x_2, x_3, x_4, x_5, x_6]^T$, with unknown parameters (variables) $k/m = x_3$ [s^{-2}], $b/m = x_4$ [s^{-1}], $c/m = x_5$ [μm.s^{-2}.V^{-1}] and $f_u/m = w = x_6$ [μm.s^{-2}]. For the optimization computational purposes the

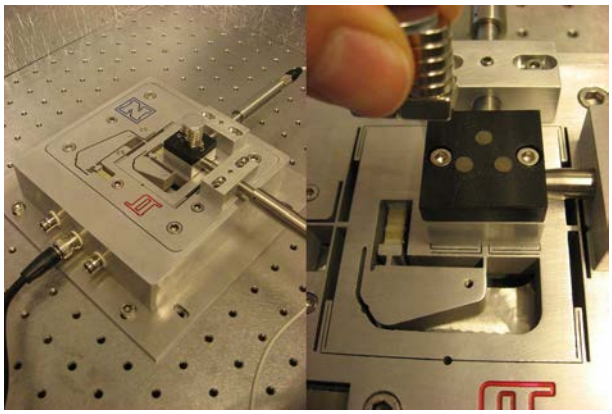

Fig. 3. Nanopositioning stage with highly resonant vibration dynamics

dynamics is partly scaled by state, input and output scales where the new variables are introduced as $x_i/s_i = x_i^s$, $z_i/s_i = z_i^s$, $u/s_u = u^s$, $y_t/s_y = y_t^s$ and $v_t/s_y = v_t^s$. The system defined by Eq.(36) is with the process noise rewritten in the nonlinear, scaled and augmented form as

$$\begin{aligned}
\dot{x}_1^s &= \frac{s_2}{s_1}x_2^s + z_1^s \\
\dot{x}_2^s &= -\frac{s_3 s_1}{s_2}x_3^s x_1^s - s_4 x_4^s x_2^s + \frac{s_5 s_u}{s_2}x_5^s u^s + \frac{s_6}{s_2}x_6^s + z_2^s \\
\dot{x}_3^s &= z_3^s; \dot{x}_4^s = z_4^s; \dot{x}_5^s = z_5^s; \dot{x}_6^s = z_6^s
\end{aligned} \tag{37}$$

where only the displacement is measurable ($s_y = s_1$)

$$y_t^s = x_{1,t}^s + v_t^s \tag{38}$$

This model formulation given by Eq. (37) is used for the EKF state estimation Eq. (18), EKF pre-filtration Eq. (30) and EKF post-filtration Eq. (32) with process noise $z^s = [z_1^s, z_2^s, z_3^s, z_4^s, z_5^s, z_6^s]^T$ defined by Eq. (10). However for the MHO model output propagation given by Eq. (28), a deterministic formulation is used where $z = 0$. The fixed numerical step for numerical integration of Eq. (37) is set to $h = 1.25.10^{-5}$[s], which gives $\frac{T_s}{h} = 8$ computational steps of the ODE solver per sampling interval.

B. Instrumentation and Experimental Data

The experiments are performed on the long-range serial-kinematic nano-positioning stage from easyLab (Figure 3), where vibration along the y axis is considered. The other used hardware is a Piezodrive PDL200 linear voltage amplifier (20 [V/V]), a ADE 6810 capacitive gauge and ADE 6501 capacitive probe from ADE Technologies to measure displacement (5 [μm/V]), and two SIM 965 programmable filters from Stanford Research Systems, used as reconstruction and anti-aliasing filters. The actuation signal and measured response was generated and recorded using a dSPACE DS1103 harware-in-the-loop board, at a sampling frequency of 10 kHz. More details about the actual hardware setup can be found in [14]. From the frequency response data, reported in [14], it was found that for the case with the payload attached, the natural frequency $f_1 = \sqrt{x_3}/2\pi = 423$[Hz] and damping ratio $\zeta_1 = x_4/2\sqrt{x_3} = 0.0146$. For the case without the payload, the natural frequency is $f_2 = 483$[Hz] and damping ratio $\zeta_2 = 0.0143$. The input excitation signal for the piezoelectric actuator is a Pseudo Random Binary Signal (PRBS). The PRBS was designed to concentrate most of its energy around the first resonant frequency of the system.

For parameter identification it is considered good practice to concentrate signal power in the frequency domains that contain peaks in the sensitivity functions [14]. This is done in order to maximize the information content of the signals used through additional filter that is chosen to be a band-pass filter [15], using a first-order high-pass filter with lower cut-off frequency of $f_{lc} = 100$[Hz], and a resonant second-order low-pass filter, with natural frequency of $f_n = 450$[Hz], and a damping ratio of $\zeta = 0.1$. The filter

$$W_p(s) = \frac{s}{s + 2\pi f_{lc}} \frac{(2\pi f_n)^2}{s^2 + 2\zeta\pi f_n s + (2\pi f_n)^2},$$

applied for the input and output data, emphasizes the frequency content close to the resonant peaks of the two configurations, with and without payload.

The MHO and EKF algorithms are tested on the data which are measured in advance. The speed signal is further computed for validation purposes by differentiating the displacement signal as

$$\dot{q}_t = \frac{y_{t+1} - y_{t-1}}{2T_s} \tag{39}$$

where T_s is a sampling period, $T_s = 10^{-4}$[s]. In this equation we use the measured displacement signal one sample ahead which is only possible with the off-line computations, in order to avoid phase loss errors.

C. Extended Kalman Filter setup

Good tuning of the EKF depends on precise information about the stochastic properties of noises. The scaling factors are set as $s_u = 5$; $s_y = 5$; $s_1 = s_y$; $s_2 = 10^4$; $s_3 = 7.10^6$; $s_4 = 7.10$; $s_5 = 8.10^5$; $s_6 = 10^5$ such that the states and parameters have approximately the same order of magnitude. The measurement noise standard deviation of displacement capacitive probe is estimated as $\sigma_y = 10^{-3}[\mu\text{m}]$ where the measurement noise covariance (matrix) is defined as

$$R_t = (\sigma_y/s_y)^2 \tag{40}$$

and set to $R_t = (10^{-3}/5)^2[\mu\text{m}^2]$. The process noise spectral density matrix is

$$Q = diag\left[\Phi_1, \Phi_2, \Phi_3, \Phi_4, \Phi_5, \Phi_6\right], \tag{41}$$

where the diagonal noise spectral densities are defined and computed as $\Phi_i = 1/T_s(\sigma_i/s_i)^2$. The standard deviation σ_i is estimated by user's assumption about the magnitude of process noise of given state or parameter of a discrete (sampled) time sequence. After some "hand tuning", the numerical values $\sigma_1 = 10^{-2}[\mu\text{m}]$, $\sigma_2 = 10^2[\mu\text{m.s}^{-1}]$, $\sigma_3 = 10^4[\text{s}^{-2}]$, $\sigma_4 = 5.10^{-2}[\text{s}^{-1}]$, $\sigma_5 = 10^3[\mu\text{m.s}^{-2}.\text{V}^{-1}]$, $\sigma_6 = 10^4[\mu\text{m.s}^{-2}]$ are found to give optimal performance. The Φ_1 spectral density is

based on standard deviation, sampling time and scale computed as $\Phi_1 = 10^4[\mathrm{s}^{-1}](0.01[\mu\mathrm{m}]/5[-])^2[\mu\mathrm{m}^2.\mathrm{s}^{-2}.\mathrm{Hz}^{-1}]$, where the other spectral densities are similarly computed. The initial state vector estimate is set to $\hat{x}_0^+ = [0/s_1, 0/s_2, 6.10^6/s_3, 70/s_4, 5.10^5/s_5, 0/s_6]^T$. The initial covariance matrix of the initial state vector estimate error is

$$P_0^+ = diag\left[\Sigma_{1,0}, \Sigma_{2,0}, \Sigma_{3,0}, \Sigma_{4,0}, \Sigma_{5,0}, \Sigma_{6,0}\right], \qquad (42)$$

where the diagonal elements are in accordance to Eq. (12) computed as $\Sigma_i = ((x_{i,0} - E[x_{i,0}])/s_i)^2$ and by initial conditions set as $\Sigma_{1,0} = (1[\mu\mathrm{m}]/5[-])^2[\mu\mathrm{m}^2]$, $\Sigma_{2,0} = (10^3/10^4)^2[\mu\mathrm{m}^2.\mathrm{s}^{-2}]$, $\Sigma_{3,0} = (1.10^6/(7.10^6))^2[\mathrm{s}^{-4}]$, $\Sigma_{4,0} = (1/(7.10))^2[\mathrm{s}^{-2}]$, $\Sigma_{5,0} = (1.10^5/(8.10^5))^2[\mu\mathrm{m}^2.\mathrm{s}^{-4}.\mathrm{V}^{-2}]$, $\Sigma_{6,0} = (1/10^5)^2[\mu\mathrm{m}^2.\mathrm{s}^{-4}]$

To prevent negative parameters, we use an ad hoc clipping strategy in which negative filtered values of parameters are set to zero.

D. Moving Horizon Observer setup

To minimize the cost function Eq. (26), Matlab's constrained optimization function `fmincon` is called. This software minimization routine is set as a nonlinear programming method known as Sequential Quadratic Programming (SQP) [16]. The first stopping criterion for this method is a relative tolerance δ_J on the cost function value where the iterations stop if $|J(x_i) - J(x_{i+1})| < \delta_J(1 + |J(x_i)|)$. The other stopping of the optimization metric is δ_x, which is a relative bound on the size of a step, meaning iterations end when $|x_i - x_{i+1}| < \delta_x(1 + |x_i|)$. These parameters are set as $\delta_J = 2.10^{-5}$ and $\delta_x = 10^{-6}$. The SQP parameters that significantly contribute to the precision of the method are maximum δ_{max} and minimum δ_{min} change in variables for finite-difference gradients. These parameters are set as $\delta_{max} = 0.1$, $\delta_{min} = 10^{-8}$. Finite differences, used to estimate gradients, are computed with central method. The number of fixed iterations and the number of function evaluations of the SQP is implicitly limited through the above mentioned parameters. The maximum number of iterations can be considered as one of the tuning parameters for the amount of filtration. The following equation for the S matrix is motivated by [12]

$$S = RP^{-1} \qquad (43)$$

Two settings of the parameter α in the cost function Eq. (26) are going to be considered: $\alpha = 1$ (MHOa) and $\alpha = 10^{-4}$ (MHOb). The length of the horizon is set to $N = 15$ that captures one oscillation period. The S matrix Eq. (43) is time-varying since $P = P^+_{t-N|t}$, Eq. (31). The values of R_t, Q and $P^+_{0|N}$ are set according to Eq. (40), (41) and (42).

The computational efficiency is a key factor when it comes to real-time processing application with DSP, CPU or FPGA. Computationally fast and efficient methods of function minimization, in the range of microseconds, based on SQP-type algorithm for real-time applications are proposed in [17].

RSE	$x_1 \times 10^{-3}$	$x_2 \times 10^3$
EKF	1.375	5.507
MHOa	0.887	5.105
MHOb	1.233	5.454

TABLE I
ROOT SQUARE ERROR

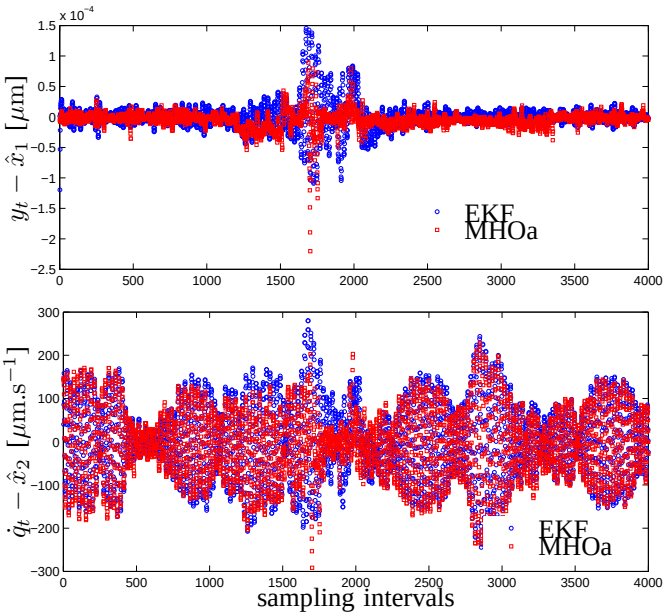

Fig. 4. Displacement and speed errors of the EKF and MHOa ($\alpha = 1$)

E. Experimental results and discussion

The quality of the algorithms is evaluated by the Root Square Error (RSE) computed for each state as

$$RSE_{x_j} = \|e_j\| = \sqrt{\sum_{t=1}^{n} e_{j,t}^2} \qquad (44)$$

where $j = 1, 2$, $n = 4000$, $e_{1,t} = y_t - \hat{x}_{1,t}$ and $e_{2,t} = \dot{q}_t - \hat{x}_{2,t}$.

The EKF and MHO are run with setups presented in previous subsections. The qualitative results are summarized through the RSE index Eq. (44) of displacement and speed in Table I. The filtering/observation accuracy of displacement and speed is in this study taken as the main criterium to evaluate the algorithms. According to this criterium the MHO, in comparison with the EKF has shown improved performance with certain trade offs. The ratio between the pre-filtered information (1st norm in Eq. (26)) and model-optimized information (2nd norm in Eq. (26)) expressed by parameter α, is one of the main tuning parameters of MHO algorithm. The value of parameter α is a tradeoff between the accuracy and parameter variance as we can further see. The comparison of EKF and MHOa is shown through the displacement and speed errors in Figure 4. The estimation of parameters and the disturbance is shown in Figure 5. In these figures the parameter $\alpha = 1$. The comparison of displacement error and speed error of EKF

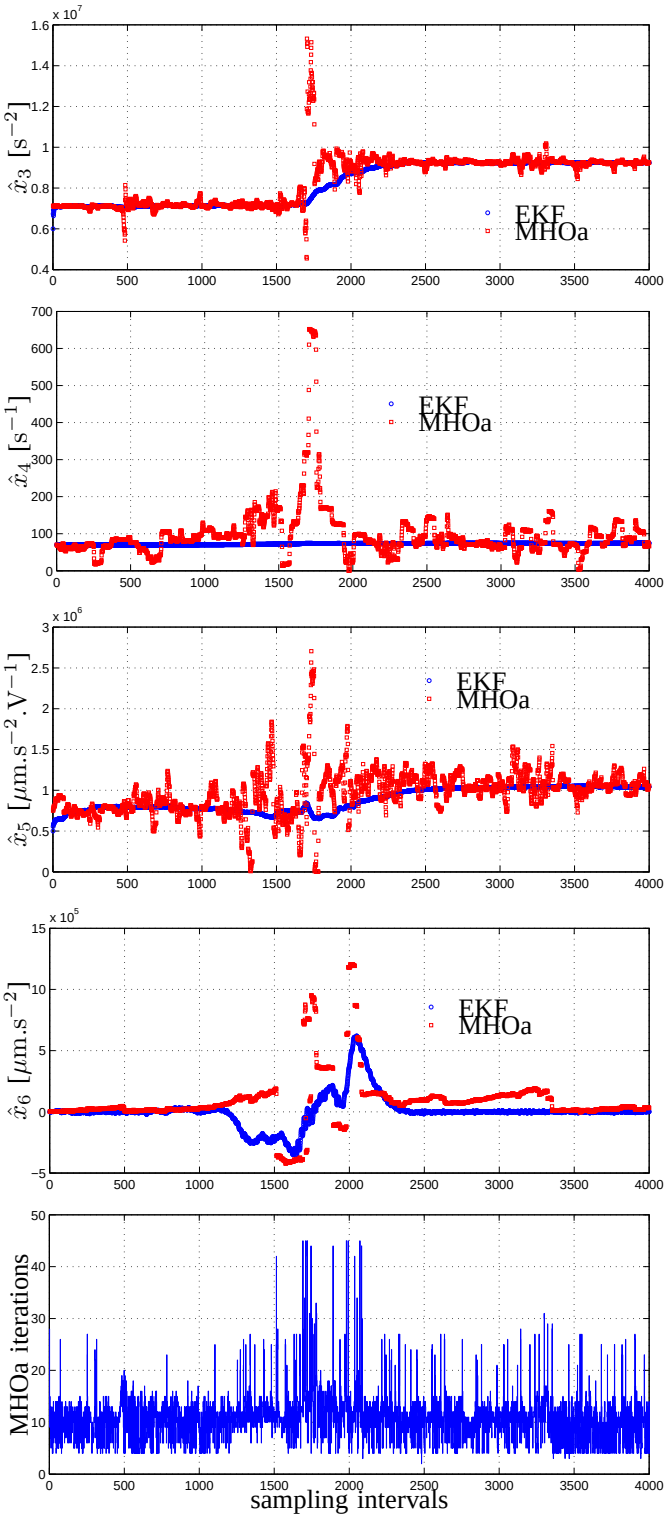

Fig. 5. Estimated parameters and disturbance of the EKF and MHOa ($\alpha = 1$)

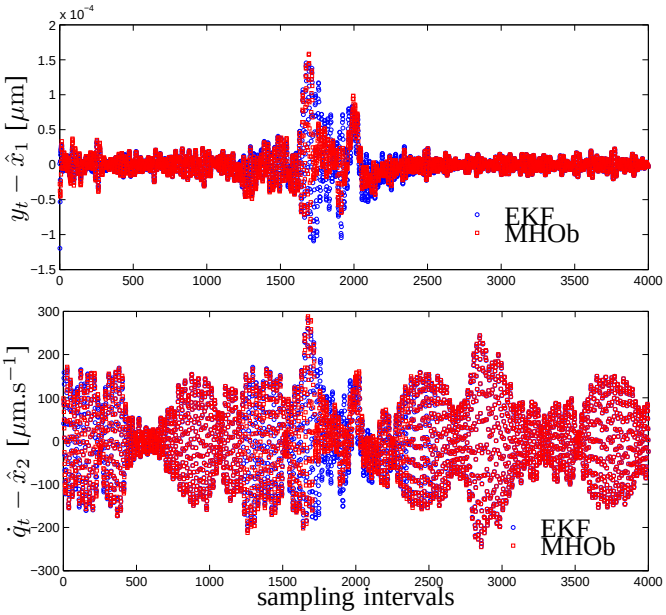

Fig. 6. Displacement and speed errors of the EKF and MHOb ($\alpha = 10^{-4}$)

and MHOb is shown in Figure 6. The estimation of parameters and the disturbance is shown in Figure 7. In these figures the parameter $\alpha = 10^{-4}$. The presented figures demonstrate faster convergence of MHO compared to the EKF during transient. The acceleration disturbance $\hat{x}_6$ is also estimated, which accounts for the force disturbance caused by the sudden removal of payload, also seen in Figure 3. Greater variance of estimated parameters given by MHOa is documented compared to MHOb. This is caused by a process noise that in pre-filtration and post-filtration part we consider to have Gaussian properties, but in moving horizon (model-optimization) part we are not modeling the uncertainty, leaving the deterministic model representation, through parameters, to reflect the unmodeled dynamics. This reflection of unmodeled higher order modes or perhaps nonlinearities in piezoelectric actuators is more evident for MHOa where much stronger trust is put on the deterministic model-based observer part through parameter α. The unmodeled process noise is closely related to a problem being ill-conditioned, when a small unmodeled disturbance causes a great change in parameters. This is highlighted in parameter estimation figures where greater variance of parameters is presented in MHOa setting in Figure 5 compared to MHOb setting in Figure 7. In this problem formulation, the α is a tradeoff between the state estimation error and parameter variance. The tuning of parameter α is a "generate and test" procedure, where $\alpha = 10^{-4}$ is the acceptable setting. The overall computational time is significantly faster in the case of MHOb when the optimization is running only when there is a potential to improve the estimates, where in the case of MHOa the iterations are running only to overfit and to model the noise through great variance of parameters.The main advantage of the MHO is that the nonlinear model leads to faster convergence of parameters and more accurate

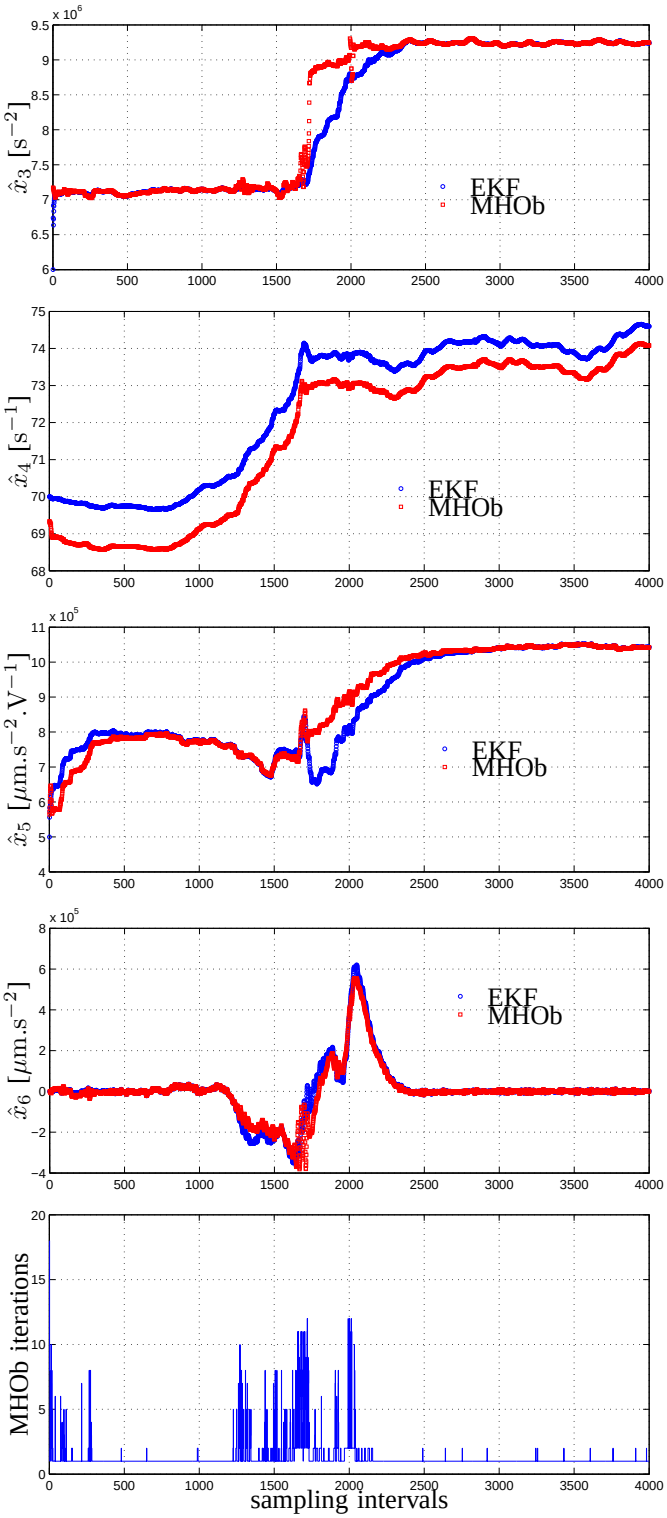

Fig. 7. Estimated parameters and disturbance of the EKF and MHOb ($\alpha = 10^{-4}$)

displacement and speed estimates during the transient.

This paper presents the state and parameter estimation of a Single-Degree-of-Freedom (SDOF) vibration dynamic system, however the proposed moving horizon observer can be applied also to a Multi-Degree-of-Freedom (MDOF) vibration system.

VII. ACKNOWLEDGMENTS

The authors wish to thank Dr. Kam K. Leang and Brian J. Kenton for providing the positioning stage, and Dr. Andrew J. Fleming for providing the amplifier used in this work.

REFERENCES

[1] S. Devasia, E. Eleftheriou, and S. Moheimani, "A survey of control issues in nanopositioning," *IEEE Transactions on Control Systems Technology*, vol. 15, no. 5, pp. 802 –823, sept. 2007.

[2] A. Gelb, J. Joseph F. Kasper, J. Raymond A. Nash, C. F. Price, and J. Arthur A. Sutherland, *Applied optimal estimation*, A. Gelb, Ed. The. M.I.T. Press, 2001.

[3] A. Corigliano and S. Mariani, "Parameter identification in explicit structural dynamics: performance of the extended Kalman filter," *Comput. Methods Appl. Mech. Engrg.*, vol. 193, pp. 3807–3835, 2004.

[4] A. Fleming, A. Wills, and S. Moheimani, "Sensor fusion for improved control of piezoelectric tube scanners," *IEEE Transactions on Control Systems Technology*, vol. 16, no. 6, pp. 1265 –1276, nov. 2008.

[5] F. Gao and Y. Lu, "A Kalman-filter based time-domain analysis for structural damage diagnosis with noisy signals," *Journal of Sound and Vibration*, vol. 297, pp. 916–930, 2006.

[6] T. Polóni, B. Rohal'-Ilkiv, and T. A. Johansen, "Damped one-mode vibration model state and parameter estimation via pre-filtered moving horizon observer," in *IFAC Symposium on Mechatronic Systems*, Boston, Massachusetts, USA, 2010.

[7] D. Sui and T. A. Johansen, "Moving horizon observer with regularisation for detectable systems without persistence of excitation," *International Journal of Control*, vol. 84, no. 6, pp. 1041–1054, 2011.

[8] A. Alessandri, M. Baglietto, and G. Battistelli, "Moving-horizon state estimation for nonlinear discrete-time systems: New stability results and approximation schemes," *Automatica*, vol. 44, no. 7, pp. 1753–1765, 2008.

[9] J. Ching, J. L. Beck, and K. A. Porter, "Bayesian state and parameter estimation of uncertain dynamical systems," *Probabilistic Engineering Mechanics*, vol. 21, pp. 81–96, 2006.

[10] R. Sajeeb, C. Manohar, and D. Roy, "A conditionally linearized Monte Carlo filter in non-linear structural dynamics," *International Journal of Non-Linear Mechanics*, vol. 44, pp. 776–790, 2009.

[11] A. N. Tikhonov and V. Y. Arsenin, *Solutions of Ill-posed Problems*. Wiley, 1977.

[12] C. V. Rao, J. B. Rawlings, and D. Q. Mayne, "Constrained state estimation for nonlinear discrete-time systems: Stability and moving horizon approximations," *IEEE Transactions on Automatic Control*, vol. 48, no. 2, pp. 246–258, 2003.

[13] J. Butcher, *Numerical Methods for Ordinary Differential Equations*. John Wiley&Sons, Ltd, 2003.

[14] A. A. Eielsen, T. Polóni, T. A. Johansen, and J. T. Gravdahl, "Experimental comparison of online parameter identification schemes for a nanopositioning stage with variable mass," in *IEEE/ASME International Conference on Advanced Intelligent Mechatronics*, Budapest, Hungary, 2011.

[15] L. Ljung, *System Identification: Theory for the User*, 2nd ed. Prentice Hall, 1999.

[16] J. Nocedal and S. J. Wright, *Numerical Optimization*, 2nd ed. Springer, 2006.

[17] B. Houska, H. J. Ferreau, and M. Diehl, "An auto-generated real-time iteration algorithm for nonlinear MPC in the microsecond range," *Automatica*, vol. 47, no. 10, pp. 2279 – 2285, 2011.